Influence of specimen geometries and drying conditions on concrete cracking in restrained elliptical ring tests

Wei Dong[1], Wenyan Yuan[2], Xiangming Zhou[3,*], Xiaoyu Zhao[4]

[1]Associate Professor, State Key Laboratory of Coastal and Offshore Engineering, Dalian University of Technology, Dalian 116024, P. R. China. E-mail: dongwei@dlut.edu.cn

[2] Postgratuate student, State Key Laboratory of Coastal and Offshore Engineering, Dalian University of Technology, Dalian 116024, P. R. China. E-mail: yuanwenyan@mail.dlut.edu.cn

[3]Professor in Civil Engineering Design, Department of Civil and Environmental Engineering, Brunel University London, Uxbridge, Middlesex UB8 3PH, United Kingdom.

(*Corresponding author) E-mail: xiangming.zhou@brunel.ac.uk

[4] Postgratuate student, State Key Laboratory of Coastal and Offshore Engineering, Dalian University of Technology, Dalian 116024, P. R. China. E-mail: zhaoxiaoyu_lv@mail.dlut.edu.cn

ABSTRACT

The restrained shrinkage elliptical ring test has been established as an efficient method for assessing the cracking potential of concrete at early ages because an elliptical ring can provide a higher degree of restraint compared with a circular one. In this study, a series of circular and elliptical concrete rings restrained by steel rings with various thicknesses were tested under top & bottom surfaces drying or outer circumferential surface drying. By comparing concrete cracking age under different geometrical and drying conditions, the effects of ring geometry, restraining steel ring thickness and drying condition on the cracking process in concrete rings were revealed. Furthermore, numerical analyses were conducted to investigate the fracture mechanism for circular and elliptical rings by applying a fictitious temperature field to simulate the shrinkage effect of concrete. It is found that the increase of steel ring thickness can enhance the degree of restraint, therefore shorten the cracking age for both circular and elliptical rings. However, the improvement is more significant for circular rings. The fracture processes under the two drying conditions, i.e. top & bottom surfaces drying and outer circumferential surface drying are completely different: for drying from outer circumferential surface, the crack initiates at the outer surface and propagates towards the inner surface; for drying from top & bottom surfaces, the crack initiates partially along the height direction at the inner circumference of a concrete ring, and propagates along the radial direction, step by step, until the crack propagates throughout the whole ring wall. In both cases, the self-restraint caused by the non-uniform shrinkage of concrete and the external restraint from the inner steel ring contribute the driving effects for crack propagation. In general, compared with circular rings, the elliptical rings demonstrate the advantage of providing a higher degree of restraint. The elliptical ring test method can, therefore, supplement the traditional circular ring test method for assessing cracking tendency of concrete with higher cracking resistance.

Keywords: Circular ring; Concrete cracking; Early-age concrete; Elliptical ring; Fictitious temperature field; Fracture of concrete; Initial fracture toughness; Restrained shrinkage; Self-restraint; Stress intensity factor

1 Introduction

The durability of concrete structures is often threatened by the restrained shrinkage cracking of concrete at early ages. Therefore, it is important to choose the appropriate laboratory test methods to assess the cracking tendency of concrete in restrained conditions prior to being used in the field. So far, several test methods have been proposed for such purpose, including the restrained uniaxial test [1-3], restrained slab test [4,5], restrained beam test [6,7], and restrained ring test [8-11]. Due to its simplicity and versatility, the restrained ring test has been widely adopted and recommended as the standard method by the American Association of State Highway and Transportation Officials (AASHTO) (i.e. AASHTO PP34-99: Standard Practice for Cracking Tendency Using a Ring Specimen) and the American Society for Testing and Materials (ASTM) (i.e. ASTM C1581/C1581M-09a: Standard Test Method for Determining Age at Cracking and Induced Tensile Stress Characteristics of Mortar and Concrete under Restrained Shrinkage).

For concrete with higher cracking resistance, it was reported that the traditional circular ring may not be able to provide high enough restraint to enable concrete ring cracking at an early age [12]. According to Moon [13], this limitation could be solved by increasing the thickness of the central restraining steel ring. However, a thicker steel ring, thus with higher stiffness, leads to smaller deformation of its inner surface, which is difficult to be detected by strain gauges that are supposed to detect the age of concrete cracking. In addition, heavy metal molds and big concrete ring specimens make it inconvenient to conduct the ring test at laboratory. In recent years, the restrained elliptical ring test was proposed and has been regarded as a supplementary method to assess the cracking potential of concrete and other cement-based materials [14-18]. In a restrained elliptical concrete ring, the first crack is expected to occur earlier compared with being in a circular ring due to the stress concentration caused by geometrical effects. Moreover, crack occurs near the major radius of an elliptical concrete ring, which is conveniently observed in experiment. Zhou et al. [15] carried out restrained shrinkage tests of a series of elliptical ring specimens with different major-to-minor radius ratios. Experimental results have proved that the elliptical rings with a geometry factor of the major-to-minor radius ratio of 2 were the most efficient in accelerating the occurrence of cracking so that shortening the ring test duration.

Based on the elliptical specimen geometry, Dong et al. [19] investigated the influence of specimen thickness on shrinkage cracking under outer circumferential surface drying. Experimental and numerical results showed that the advantage of the elliptical geometry is obvious in thin concrete rings (i.e. with the ring thickness of 37.5mm) but invalid in thick concrete rings (i.e. with ring thickness of 75mm), because of the greater self-restraint caused by non-uniform shrinkage along the radial direction. In fact, the non-uniform shrinkage in concrete results in the self-restraining effect, which contribute the driving forces for crack evolution in concrete together with the restraint from the inner steel ring. For the purpose of the assessment of cracking potential in concrete under externally restrained condition, it is more appropriate to reduce the effect of self-restraint, which can be achieved by decreasing the diffusion distance in the concrete ring. Upon this point, drying from top & bottom surfaces was investigated for an extension of standard ring test methods recommended by AASHTO and ASTM in some studies [20-25] in which drying is usually from outer circumferential surface only.

Under drying from the top & bottom surfaces, the moisture diffuses simultaneously from the two symmetrically exposed surfaces (i.e. the top and bottom surfaces) of a concrete ring so that the moisture diffusion distance is half of the height of the ring specimen. However, it should be noted that, although uniform shrinkage along the radial direction can be obtained, non-uniformity still exists along the height direction. Particularly, the non-uniform shrinkage along the height affects the crack initiation position and propagation direction in concrete, which shows a completely different fracture process compared with the case of drying from outer circumferential surface in ring test [20]. Therefore, to reinforce the advantage of the elliptical geometry, these influential factors, i.e., specimen geometry, thickness of steel ring and drying condition, should be investigated comprehensively, so that a more effective test method can be recommended to assess the cracking potential of concrete under restrained shrinkage conditions.

In line with this, a series of restrained circular and elliptical ring specimens were tested under drying from top & bottom surfaces, and outer circumferential surface, respectively. In addition, the influence of restraining steel ring thickness was investigated through examining two thicknesses, i.e. 12.5 mm and 19.5 mm. By comparison of concrete cracking age under different conditions, the effects of ring geometry, steel ring thickness and drying condition on crack initiation and propagation were revealed. Furthermore, a numerical analysis was conducted to investigate the fracture mechanism for circular and elliptical rings by applying a fictitious temperature field to simulate the shrinkage effect of concrete. It is expected that the research conducted in this paper can reveal the influential factors of the elliptical ring specimen on concrete cracking so that more appropriate test condition can be selected for assessing cracking potential of concrete under restrained shrinkage.

2 Experimental programs

The basic mechanical, fracture properties and free shrinkage of concrete were measured. The mix proportions for the concrete used in the test were 533 kg/m^3 : 800 kg/m^3 : 800 kg/m^3 : 267 kg/m^3 (cement: sand: aggregate: water) and the maximum size of crushed gravel aggregate was 10 mm. After curing in a normal laboratory environment for 24 h, the specimens were demoulded and moved into an environmental chamber set at 23°C and 50% relative humidity (RH) for curing until the designated age of testing or cracking in cases of the ring test.

2.1 Material Properties

Mechanical and fracture properties, including elastic modulus E, splitting tensile strength f_t, fracture energy G_f, and initial fracture toughness $K_{\mathrm{IC}}^{\mathrm{ini}}$, of concrete for making ring specimens in this study, were measured at 1, 3, 5, 7, 14, 21 and 28 days. The elastic modulus E and splitting tensile strength f_{t} were measured by the method recommended by GB/T 50081-2002 (Standard for Test Method of Mechanical Properties on Ordinary Concrete). The fracture energy G_{f} was measured by the standard method recommended by RILEM Committee FMC50 (Determination of the Fracture Energy of Mortar and Concrete by Means of the Three-Point Bend Test). Three specimens were prepared for measuring each mechanical property of concrete at each designated age. Experiment data of concrete at various ages were fitted to a continuous function through regression analyses, which are shown in Figs. 1 (a) to (d). Accordingly, the age-dependent materials properties of concrete from 1 to 28 days can be obtained through Eqs. 1 to 4, in which t is the age of concrete (Unit: days).

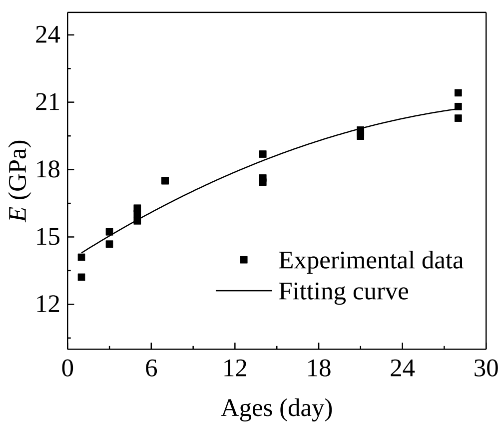

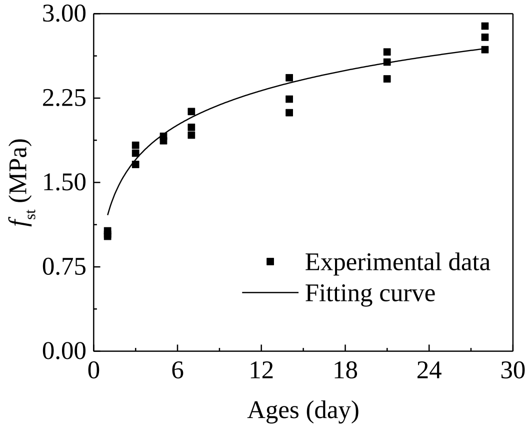

(a) E at various ages (b) f_t at various ages

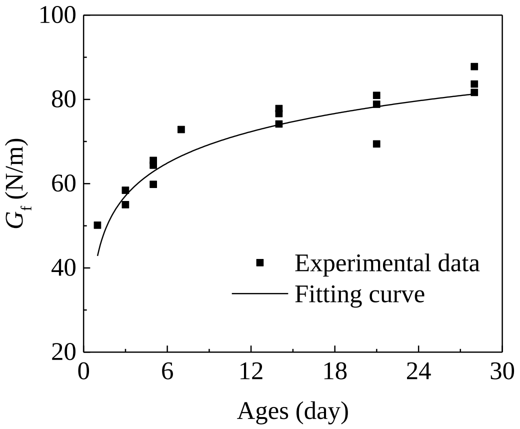

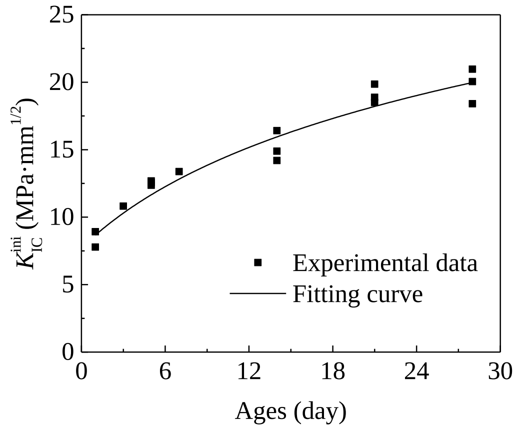

(c) G_f at various ages (d) K_{IC}^{ini} at various ages

Fig. 1. Relationship of materials properties at various ages

$$E(t) = 13.8973 + 0.4t - 0.0056t^2 \qquad (t \le 28) \tag{1}$$

$$f_t(t) = 1.224 + 0.44 \times \ln(t - 0.0318) \qquad (t \le 28) \tag{2}$$

$$G_f(t) = 41.39 + 10.35 \times \ln(t - 0.326) \qquad (t \le 28) \tag{3}$$

$$K_{IC}^{ini}(t) = -0.301 + 0.26 \times \ln(t + 0.272) \qquad (t \le 28) \tag{4}$$

2.2 Restrained Ring Tests

The ring specimens tested in this study can be divided into two groups based on drying condition: (1) outer circumferential surface drying (out) and (2) top & bottom surface drying (t&b). Meanwhile, two types of ring geometries, i.e. circular and elliptical, were investigated in this study, which are illustrated in Fig. 2. Here, R_0 denotes the inner radius of a circular concrete ring, and R_1 and R_2 denote the major and minor inner radii of the elliptical concrete ring, respectively. In this study, R_0, R_1 and R_2 were chosen as 150 mm, 150 mm and 75 mm, respectively. In addition, the thickness of the steel ring is varied as 12.5 mm and 19.5 mm for both types of ring geometries. The details of the circular (*c*) and elliptical (*e*) ring specimens tested in this study are listed in Table 1. A test specimen identifying system was adopted. The test identifier is presented as *c*-(or *e*-)out-*m*-37.5 for outer circumferential surface dried specimens and *c*-(or *e*-)*t*&*b*-*m*-*n* for top and bottom surface dried specimens in which *c* stands for circular specimens and *e* for elliptical specimens, *m* denotes the thickness (in mm) of the central restraining ring and *n* stands for the concrete ring height (in mm). Taking Specimen c-t&b-12.5-30 as an example, "*c*" denotes a circular ring geometry, "*t&b*" denotes drying from top & bottom surfaces, "12.5" donates a steel ring thickness of 12.5 mm, and "30" denotes a concrete ring height of 30 mm. It should be noted that, in the case of drying from outer circumferential surface, the last number 37.5 in Specimen c-out-12.5-37.5 denotes a concrete ring thickness of 37.5 mm.

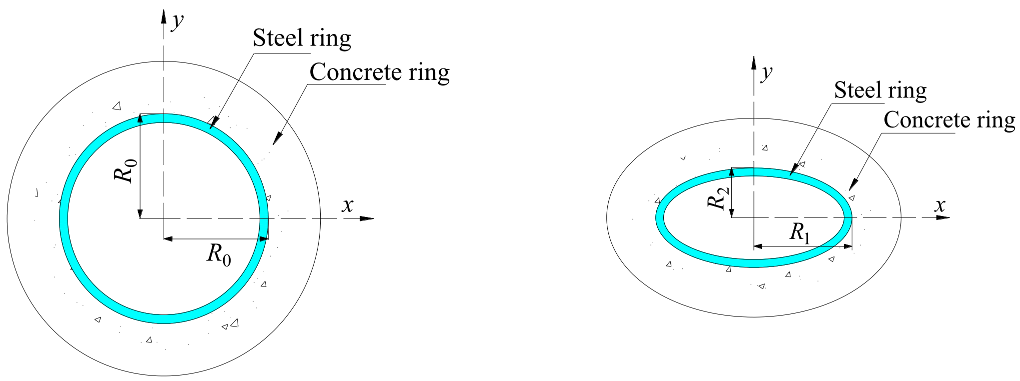

(a) Circular ring (b) Elliptical ring

Fig. 2. Diagrams of the restrained circular and elliptical ring specimens

Table 1. Geometries of ring specimens and corresponding cracking ages

Drying direction	Specimen	Height (mm)	Steel ring thickness (mm)	Concrete ring thickness (mm)	Cracking ages (days) Exp.	Cracking ages (days) Num.
Outer surface	c-out-12.5-37.5	75	12.5	37.5	16	12
	e-out-12.5-37.5				12	9
	c-out-19.5-37.5		19.5		13	9
	e-out-19.5-37.5				10	8
Top and bottom surfaces	c-t&b-12.5-30	30	12.5	75	19	18
	e-t&b-12.5-30				14	15
	c-t&b-19.5-30		19.5		16	16
	e-t&b-19.5-30				12	13
	c-t&b-12.5-50	50	12.5	75	24	25
	e-t&b-12.5-50				21	19
	c-t&b-19.5-50		19.5		20	22
	e-t&b-19.5-50				18	17

In each ring test, the central restraining steel ring had four strain gauges attached on its inner surface. Finally, a data acquisition system was used to detect the age of the first crack in the concrete ring by a sudden drop of strain in the steel ring picked by the attached strain gauges. Fig. 3 (a) shows the drop in strain detected from specimen c-t&b-12.5-30 over the test period and Fig. 3(b) accordingly illustrates the crack on it.

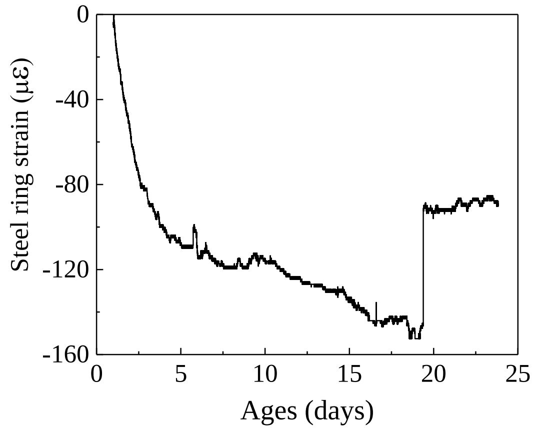

(a) Variation of strains over the ages (b) Crack in the specimens

Fig. 3. Experiment results of Specimen c-t&b-12.5-30

The average cracking ages for all ring specimens tested are also listed in Table 1. It can be seen that elliptical ring specimens cracked up to 4 days earlier than the corresponding circular ring specimens, which demonstrated the advantage of the elliptical geometry in accelerating the occurrence of cracking. For the 30 mm high ring specimens under top & bottom surface drying, both circular and elliptical ring specimens with a thicker steel ring, i.e. with the thickness of 19.5mm, cracked earlier than those with a thinner steel ring, i.e. with the thickness of 12.5mm. Moreover, the differences in cracking ages were about 3 days and 2 days for the circular ring geometry and elliptical ring geometry, respectively. It means that a thicker steel ring can enhance the degree of restraint to both circular and elliptical ring specimens. Making a comparison between 30 mm and 50 mm high concrete ring specimens, the 30 mm high ring specimens cracked earlier than the 50 mm high ring specimens. This may be as a result of a more significant non-uniform shrinkage along the height direction, which is discussed later in this paper.

2.3 Free Shrinkage Tests

To take into account the shrinkage of the concrete, the free shrinkage tests were carried out using prismatic specimens. Furthermore, in order to match the drying conditions in the ring tests, including the drying direction and humidity diffusion distance, three series of free shrinkage prism tests with specimen sizes of 300 mm × 75 mm × 37.5 mm, 300 mm × 75 mm × 30 mm and 300 mm × 75 mm × 50 mm were conducted to measure the free shrinkage strain of concrete. For the prisms of 300 mm × 75 mm × 37.5 mm, only a 300 mm × 75 mm surface was exposed for drying; the other surfaces were sealed using a double-layer aluminium tape to match rings drying from the outer surface of a concrete ring specimen. For the prisms of 300 mm × 75 mm × 30 mm and 300 mm × 75 mm × 50 mm, the specimens were dried from two symmetrically exposed 300 mm × 75 mm surfaces and the other surfaces were sealed using a double-layer aluminium tape to match the scenario that concrete rings were dried from top & bottom. The magnitudes of free shrinkage were measured using mechanical dial gauges (see Fig. 4(a)) and the result was recorded twice a day at regular intervals.

By fitting the measured data, free shrinkage strains at different ages can be derived, which are graphically presented in Fig. 4 (b).

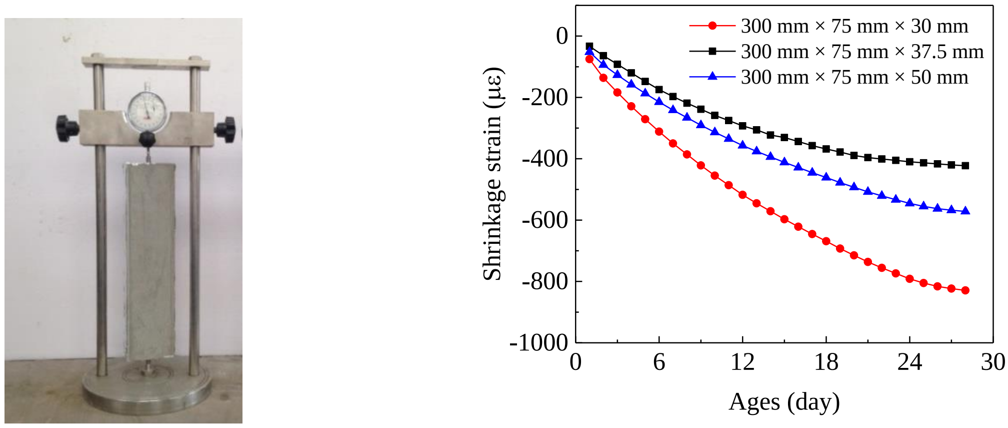

(a) Free shrinkage test set-up (b) Free shrinkage strain

Fig. 4. Free shrinkage test.

3. Numerical simulation

3.1 Derivation of the fictitious temperature field

In this study, numerical analyses were carried out using ANSYS finite element codes to investigate the crack initiation and propagation process for all ring specimens listed in Table 1. In the numerical analyses, the fictitious temperature field, derived from the free shrinkage test, was applied in the numerical model to simulate the mechanical effect of concrete shrinkage. According to Moon et al. [26], the relationship between moisture distribution and shrinkage strain can be regarded as being linear when the relative humidity (RH) is greater than 50%. In this study, the moisture distribution in a concrete specimen can be calculated from Eq. (5), which was proposed by Weiss et al. [22]

$$H\left(x,t\right)=H_{INTERNAL}-(H_{INTERNAL}-H_{EXPOSED})\left(10^{-(A_1D+A_2)t^{(B_2+B_1 ln(D))}\frac{x}{D}}\right) \quad (5)$$

where $H(x,t)$ is the relative humidity at the depth x from the drying surface, H_{INTERNAL} is the internal relative humidity of the concrete specimen, which was assumed to be 100% because the specimen was completely sealed in this study; $H_{EXPOSED}$ is the relative humidity at the exposed surface of the specimen, which was the same as the relative humidity in environment and determined as 50% in this study. According to Weiss et al. [22], the coefficients A_1, A_2, B_1 and B_2 in Eq. (5) were determined to be 0.2007, -1.0455, 0.0865 and -0.9115, respectively. D is the distance of between the designated concrete element and the drying surface. In addition, the coefficient of thermal expansion, 10×10^{-6}/℃, was introduced to establish the relationship of the temperature and shrinkage strain in the concrete specimens. By establishing the relation between the drying shrinkage strain from experiment and the strain caused by the temperature decrease, the fictitious temperature fields can be derived for the three cases, i.e., 37.5 mm-thick prism drying from single surface, 30 mm- and 50 mm- thick prisms drying from two symmetrical surfaces, which are illustrated in Fig. 5. The three fictitious temperature fields were accordingly applied to the rings with the three geometrical and drying conditions, i.e. 37.5 mm-thick rings drying from outer surfaces, 30 mm- and 50 mm- high rings drying from top & bottom surfaces.

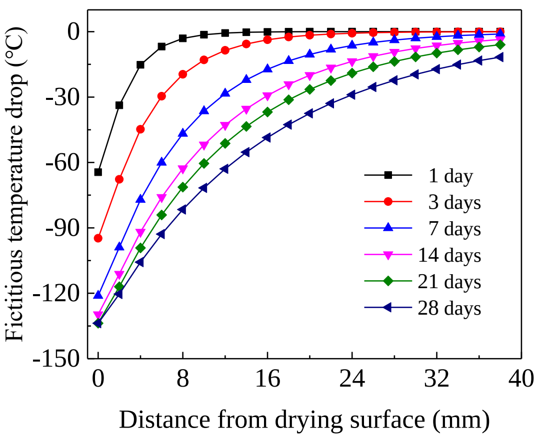

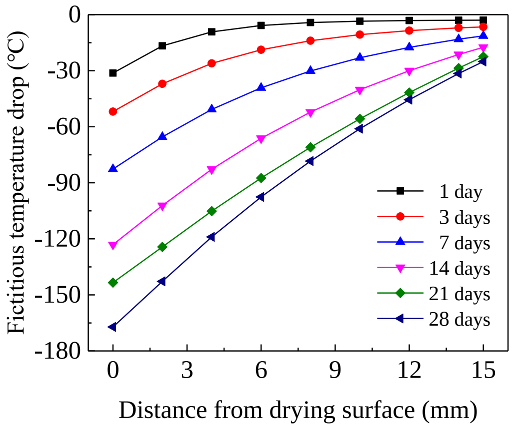

(a) Drying from outer surface: 37.5 mm thick

(b) Drying from top & bottom: 30 mm high

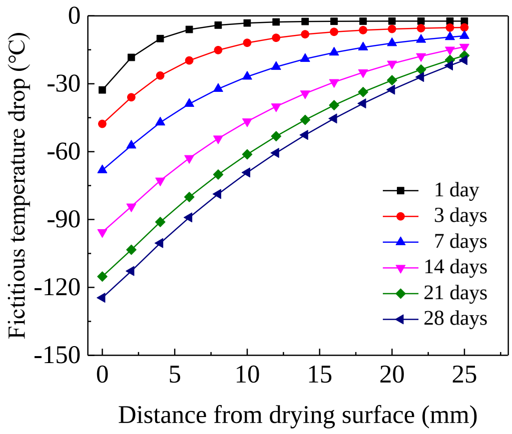

(c) Drying from top & bottom: 50 mm high

Fig. 5. Fictitious temperature field derived from the experiment

3.2 Fracture model in numerical simulation

A fictitious crack model [27] was introduced in the fracture analysis to characterize the nonlinear property of concrete by applying a cohesive force to the fracture process zone (FPZ). The bilinear expression for the relationship of cohesive stress (σ) and crack opening displacement (w) in concrete was used in the numerical simulation. According to Peterson [28], σ at the starting point of σ-w relationship with zero crack opening displacement is f_t, and w at the ending point with zero cohesive stress is $3.6G_f/f_t$. Moreover, σ and w corresponding to the breakpoint in the bilinear softening relationship equal to $f_t/3$ and $0.8G_f/f_t$, respectively. Therefore, the σ-w relationship can be determined through giving fracture energy G_f and tensile strength of concrete f_t, which can be derived from the fit expressions (i.e. Eqs. (2) and (3), respectively).

Furthermore, a concrete crack propagation criterion based on the initial fracture toughness [29, 30] was introduced in the numerical model to determine the crack initiation and propagation in the concrete rings subjected to restrained shrinkage. The criterion can be described as: a crack begins to propagate when the difference between the stress intensity factors (SIFs) caused by the shrinkage effect, $K_{\mathrm{I}}^{\mathrm{S}}$, and by the cohesive stress, K_{I}^{σ}, exceeds the initial fracture toughness of concrete, $K_{\mathrm{IC}}^{\mathrm{ini}}$. The criterion can be formulated as follows:

$$K_{\mathrm{I}}^{\mathrm{S}} - K_{\mathrm{I}}^{\sigma} < K_{\mathrm{IC}}^{\mathrm{ini}}, \text{ crack does not propagate} \tag{6}$$

$$K_{\mathrm{I}}^{\mathrm{S}} - K_{\mathrm{I}}^{\sigma} = K_{\mathrm{IC}}^{\mathrm{ini}}, \text{ crack is in the critical state} \tag{7}$$

$$K_{\mathrm{I}}^{\mathrm{S}} - K_{\mathrm{I}}^{\sigma} > K_{\mathrm{IC}}^{\mathrm{ini}}, \text{ crack propagates} \tag{8}$$

Firstly, a 2 mm-long initial crack was set at the potential cracking position, which can be determined through the maximum circumferential tensile stress in the concrete ring. In order to reduce the impact of the artificially pre-set crack on the fracture analysis, the cohesive force was applied on the crack according to the crack opening displacement under the fictitious temperature field. In this case, the SIF of $K_{\mathrm{I}}^{\mathrm{S}}$ at the tip of the pre-crack can be calculated using the displacement extrapolation method, and the SIF of K_{I}^{σ} can also be derived by means of the bilinear *σ-w* relationship. Thus, the crack propagation status can be determined by comparing $K_{\mathrm{I}}^{\mathrm{S}}$ - K_{I}^{σ} and $K_{\mathrm{IC}}^{\mathrm{ini}}$. If Eq. (8) is satisfied, the crack will propagate, and a new numerical model will be re-established with a crack length increment of 2 mm. If not, the fictitious temperature field corresponding to the next time step (in this case next day) will be adopted, and the SIFs of $K_{\mathrm{I}}^{\mathrm{S}}$, K_{I}^{σ} and $K_{\mathrm{IC}}^{\mathrm{ini}}$ will be re-calculated until Eq. (8) is satisfied. The elastic modulus of concrete was reduced by 40% to consider the creep effect of concrete [13, 31]. By carrying out the abovementioned iteration process, the whole fracture process of the concrete ring under restrained shrinkage condition can be simulated. Fig. 6 illustrates the mesh of specimen *e-out-12.5-37.5* when the crack propagation length is 15 mm. The predicted cracking ages (see Table 1) show reasonable agreements with the experimental results, which validates the proposed numerical method in this study.

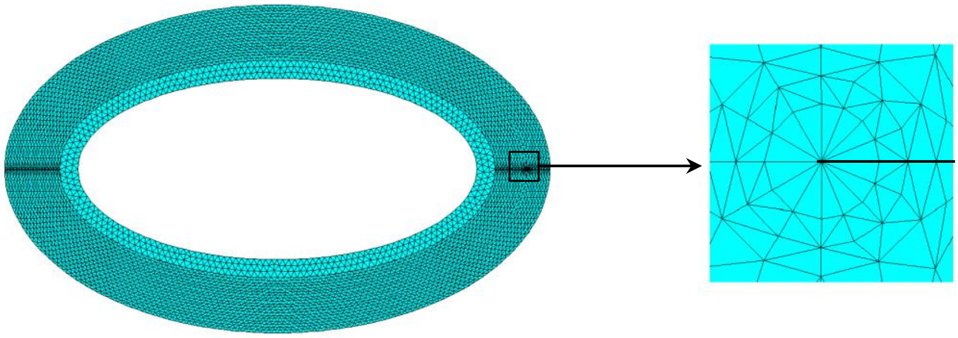

Fig. 6. Mesh of Specimen *e-out-12.5-37.5*

4. Results and discussions

4.1 Effect of drying direction on crack initiation and propagation in concrete rings

To have a deep understanding on the fracture process of restrained concrete rings under drying from the outer circumferential and top & bottom surfaces, it is significant to clearly clarify the crack initiation and propagation in the two drying conditions. In this study, the positions of initial cracks were determined by means of maximum circumferential tensile stresses in the concrete rings. Figs. 7 (a) to (f) present the circumferential tensile stress contours for the ring specimens with 12.5 mm-thick steel rings at the age of 15 days.

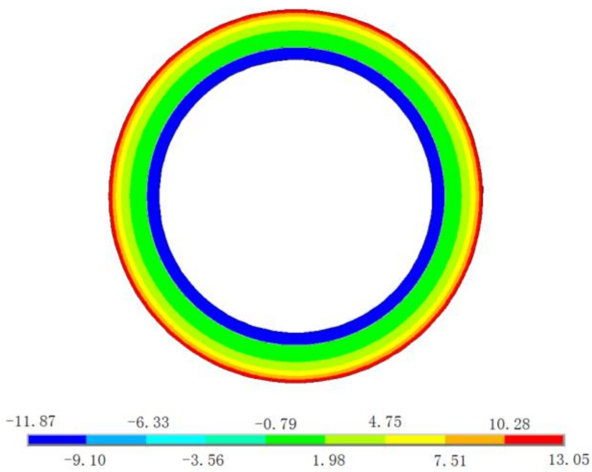

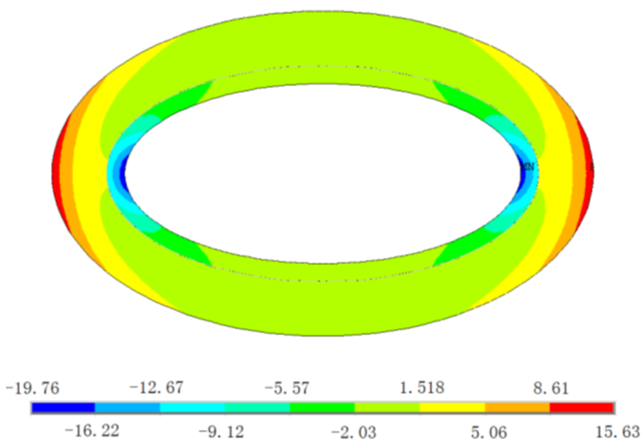

(a) Specimen c-out-12.5-37.5 (b) Specimen e-out-12.5-37.5

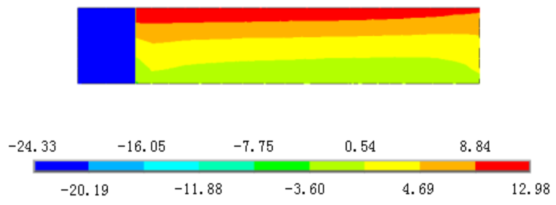

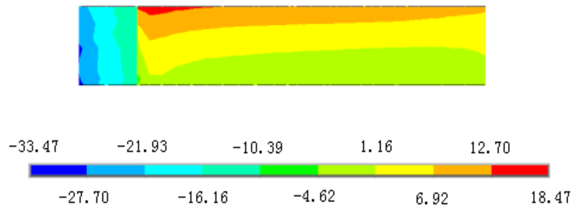

(c) Specimen c-t&b-12.5-30 (along the height) (d) Specimen e-t&b-12.5-30 (along the height)

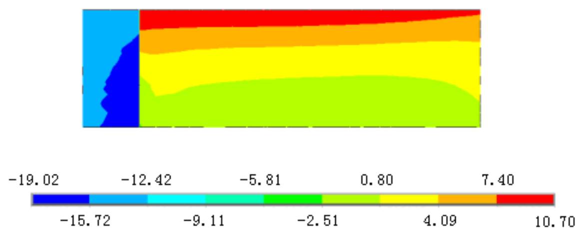

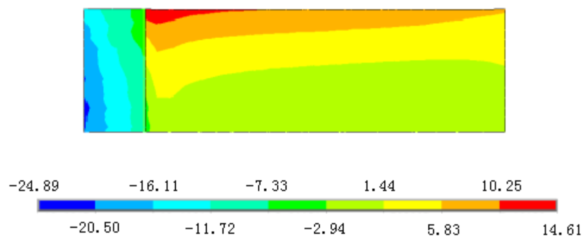

(e) Specimen c-t&b-12.5-50 (along the height) (f) Specimen e-t&b-12.5-50 (along the height)

Fig. 7. Stress contour of ring specimens at the age of 15 days

For the ring specimens dried from their outer circumferential surface, the stresses are the same along the height direction so that their distributions can be adequately illustrated in plane. It can be seen from Figs. 7(a) and (b) that the maximum circumferential stress occurs at the outer surfaces for both the circular and elliptical rings. In the case of the circular ring, the maximum tensile stress is distributed equally at its outer surface allowing the crack to initiate randomly at any position on the outer circumferential surface. By contrast, in the case of the elliptical ring, the maximum stress value occurs near the major radius of the elliptical ring, indicating that a potential crack can appear at that corresponding position.

For the specimens drying from top & bottom surfaces, the stresses vary along the height direction due to the effect of non-uniform shrinkage so that their distributions in the cross-sections are presented. It should be noted that only the half of specimen height is considered due to the symmetries of geometry about the median surface and drying condition. Figs. 7(c)-(f) show the stress distribution of cross section (random along circumference for a circular ring and along the major radius for an elliptical ring) for the ring specimens under drying from top and bottom surfaces. In these figures, the left and right rectangular block represents the steel ring and concrete ring, respectively. It can be seen from Figs. 7(c) to (f) that the tensile stress distributions are hierarchical in intensity along the height direction. The tensile stress reaches its highest at the top surface and decreases along the height direction down to median surface of the ring specimen. In this manner, it can be predicted that a crack will most likely occur at the top left and bottom left corners of the cross-section for both the circular and elliptical specimens with different heights.

After the initial crack position is determined, it is necessary to analyze the crack propagation process under restrained shrinkage. The cracking ages (see Table 1) of the concrete rings were predicted using the aforementioned numerical procedure. Figs. 8(a) to (f) show the relationships of $K_{\mathrm{I}}^{\mathrm{S}}$ - K_{I}^{σ} and $K_{\mathrm{IC}}^{\mathrm{ini}}$ in the specimens at their corresponding cracking age. According to the analyses of the stress distributions, the crack will initiate at the outer surface and propagate towards the inner surface for the specimens drying from their outer circumference. From the results in Figs. 8(a) and (b), it can be seen that the SIFs of $K_{\mathrm{I}}^{\mathrm{S}}$ - K_{I}^{σ} keep increasing and always remain greater than $K_{\mathrm{IC}}^{\mathrm{ini}}$ for both the circular and elliptical specimens at their corresponding cracking age. Therefore, it can be concluded for the specimens drying from outer circumferences, the cracks will propagate throughout the cross-sections once they initiate. In contrast, according to the results in Figs. 8(c) to (f), the SIFs of $K_{\mathrm{I}}^{\mathrm{S}}$ - K_{I}^{σ} increase firstly and then decrease. However, except for Specimen c-t&b-12.5-50, the values of $K_{\mathrm{I}}^{\mathrm{S}}$ - K_{I}^{σ} in these samples are greater than $K_{\mathrm{IC}}^{\mathrm{ini}}$, indicating that the crack can propagate through its horizontal section step by step until the whole crack section is formed at the cracking age. Even for Specimen c-t&b-12.5-50, the crack can form completely at the next age, i.e. at the 25$^{\mathrm{th}}$ day. In summary, the strain decrease of the steel ring observed in the ring test means a crack initiates as well as approximately propagates throughout the entire wall of a concrete ring specimen.

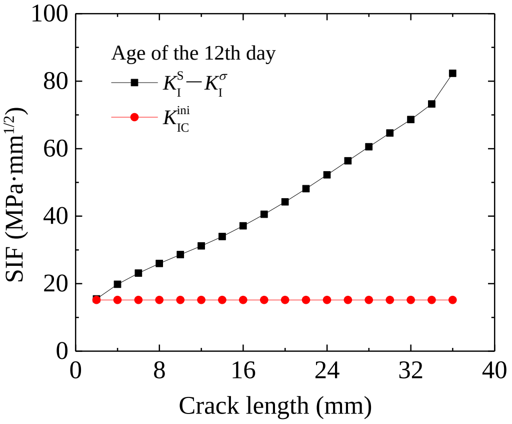

(a) Specimen c-out-12.5-37.5

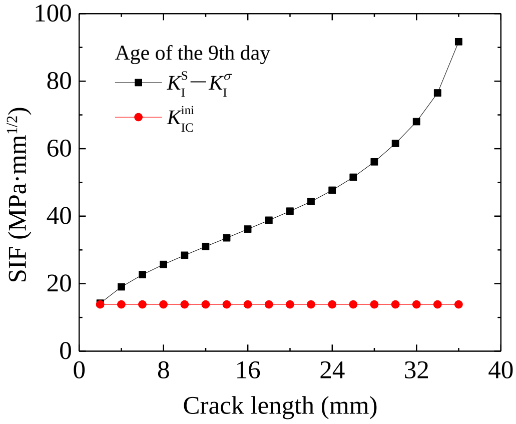

(b) Specimen e-out-12.5-37.5

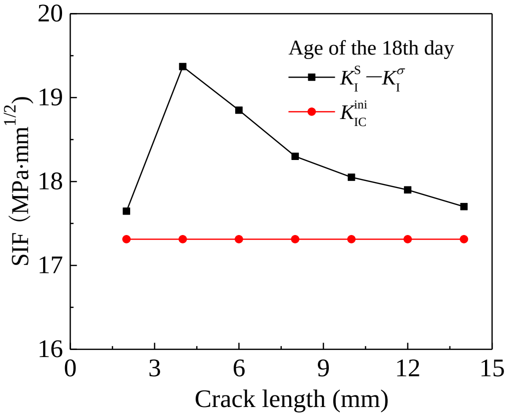

(c) Specimen c-t&b-12.5-30

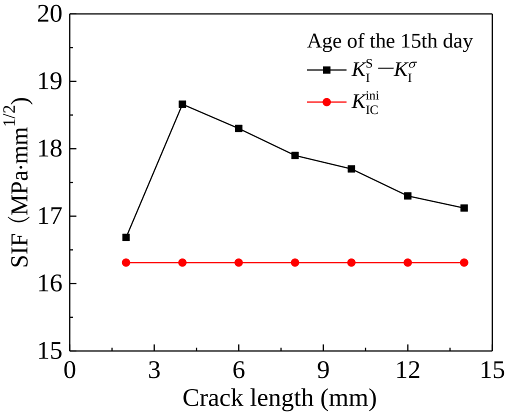

(d) Specimen e-t&b-12.5-30

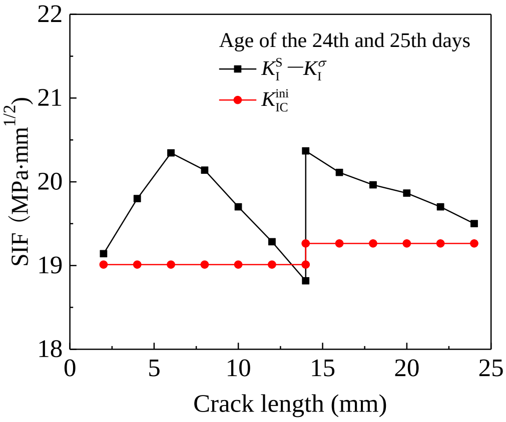

(e) Specimen c-t&b-12.5-50

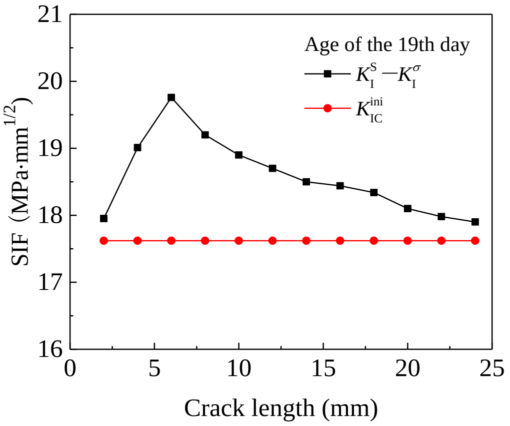

(f) Specimen e-t&b-12.5-50

Fig. 8. Relationships of K_I^S - K_I^σ and K_{IC}^{ini} at the cracking ages

4.2 Effects of ring geometry and thickness of steel ring on cracking ages

Since a crack approximately propagates throughout the cross-section very shortly after its initiation, it is valuable to investigate the effects of ring geometry and thickness of steel ring on the cracking age under restrained shrinkage. To quantify the effects of the ring geometry, the relationships of $K_{\mathrm{I}}^{\mathrm{S}}$ - K_{I}^{σ} and $K_{\mathrm{IC}}^{\mathrm{ini}}$ at various ages were investigated for all specimens used in this study, which are shown in Figs. 9(a) to (f). It can be seen, for the specimens drying from outer circumferences, the elliptical geometry with a 12.5 mm-thick steel ring can provide a more significant restraining effect compared with the circular one, resulting in an earlier cracking age (the difference between the predicted cracking ages of circular and elliptical rings is 3 days). However, with the increase of steel ring thickness from 12.5 mm to 19.5 mm, the advantage of the elliptical geometry becomes less obvious (the difference of predicted cracking ages in circular and elliptical rings is only 1 day). It indicates that the increase of the steel ring thickness provides an effective contribution to the restraining effect in the circular and elliptical rings under drying from the outer circumferential surface. However, in the case of drying from top & bottom surfaces, the elliptical geometry is advantageous to the specimens with different thicknesses. The predicted cracking ages in elliptical geometry are 3, 3, 6 and 5 days earlier than the ones in circular geometry for the cases of t&b-12.5-30, t&b-19.5-30, t&b-12.5-50 and t&b-19.5-50, respectively.

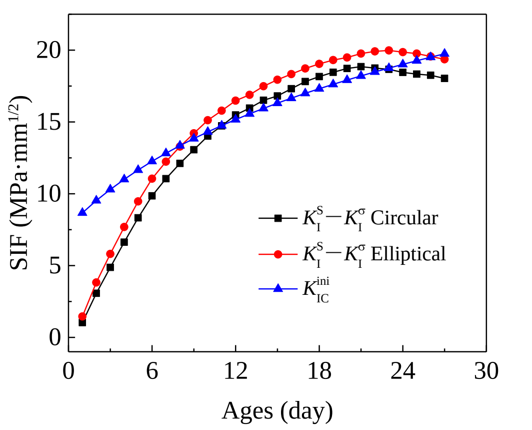

(a) Specimens c/e-out-12.5-37.5

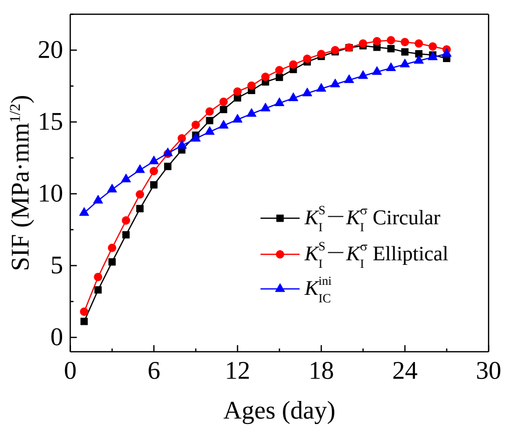

(b) Specimens c/e-out-19.5-37.5

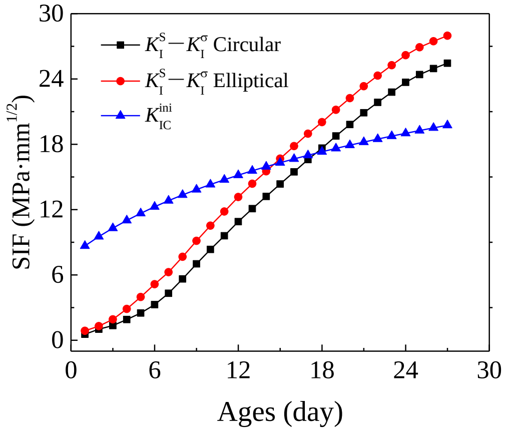

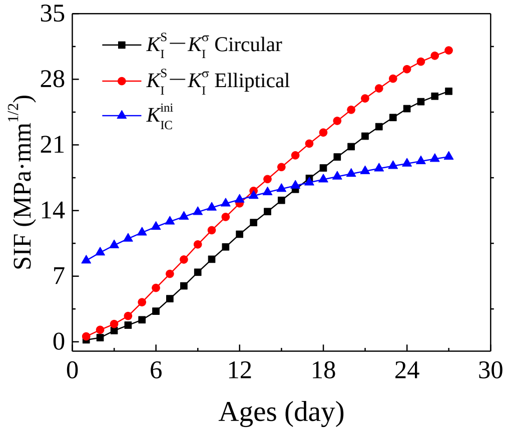

(c) Specimens c/e-t&b-12.5-37.5 (d) Specimens c/e-t&b-19.5-37.5

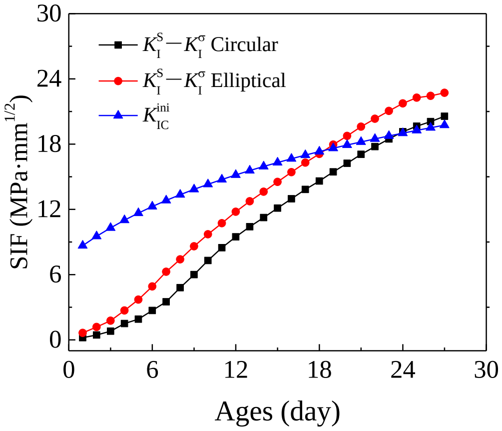

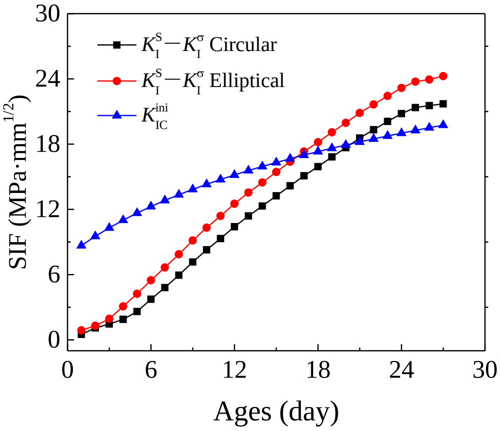

(e) Specimens c/e-t&b-12.5-37.5 (f) Specimens c/e-t&b-19.5-37.5

Fig. 9. Relationships between K_I^S - K_I^σ and K_{IC}^{ini} on various ages

In order to further investigate the effect of the steel ring thickness on the cracking age of concrete in the ring test, Fig. 10 illustrate the ratios of $K_{I\,steel}^S$ to K_I^S in the crack propagation processes. Here, $K_{I\,steel}^S$ is the SIF caused by the restraint from inner steel ring and K_I^S is the SIF caused by the total restraints, i.e. the combined restraint from the inner steel ring and the non-uniform shrinkage (i.e. self-restraint) of concrete. It is shown that, in the case of the circular geometry, the increase of the steel ring thickness can slightly enhance the proportion of the restraint from steel ring in the total restraint. In contrast, the increase of the steel ring thickness for the elliptical geometry has almost no contribution to the improvement of the restraining effect. The ratios of $K^{S}_{I\,steel}$ to K^{S}_{I} keep increasing as crack propagates. However, the crack will propagate throughout the whole cross-section once it is initiated, so the values of $K^{S}_{I\,steel}$ to K^{S}_{I} at the cracking ages are more important in determining the cracking potential in restrained shrinkage conditions. Based on the latter point, Table 2 lists the ratios of $K^{S}_{I\,steel}$ to K^{S}_{I} at the cracking ages for all ring specimens investigated in this study. It is interesting to note that the ratios of $K^{S}_{I\,steel}$ to K^{S}_{I} are less than 50% for all specimens, signifying that the fractures are not dominated by the restrained shrinkage but rather by the self-restraint caused by the non-uniform shrinkage in concrete. It should be noted that the moisture distribution in concrete has a significant effect on the analysis of the fracture mechanism in the ring tests. The moisture distributions in this study are from experimental investigations, in which several humidity sensors are placed at different drying depths to measure the relative humidity, and the moisture distribution is obtained by curve fitting the experimental data. In fact, the calculation of the moisture gradient may be not as straightforward as that presented in Eq. (5). Hence, for a more meaningful determination of the fracture mechanism, an accurate derivation of the moisture distribution is significant in the fracture analyses of concrete ring tests and thus, reserved for a future study.

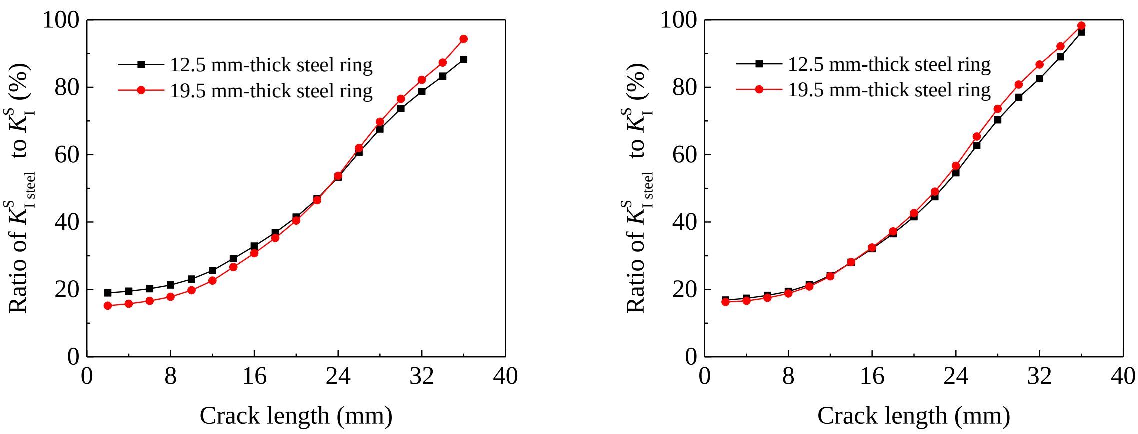

(a) Specimens c-out-12.5/19.5-37.5

(b) Specimens e-out-12.5/19.5-37.5

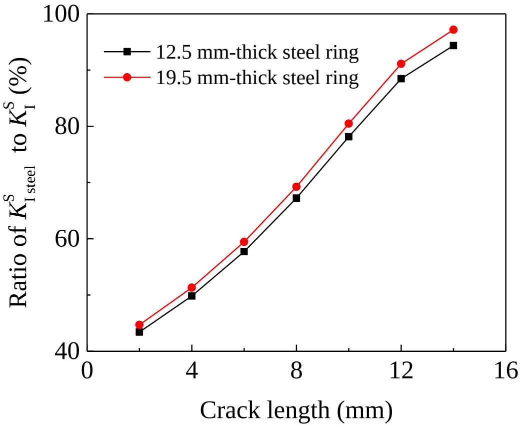

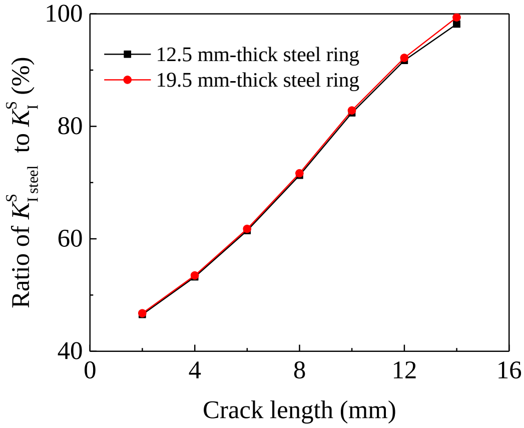

(c) Specimens c-t&b-12.5/19.5-30

(d) Specimens e-t&b-12.5/19.5-30

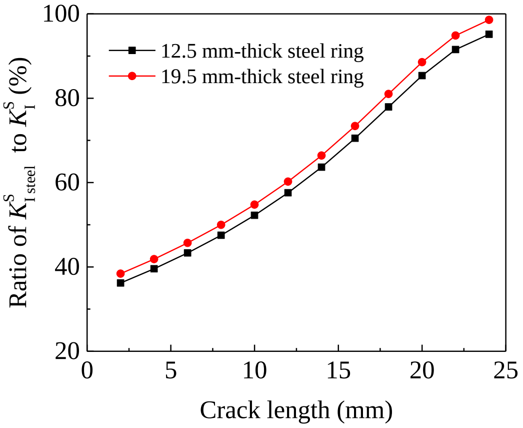

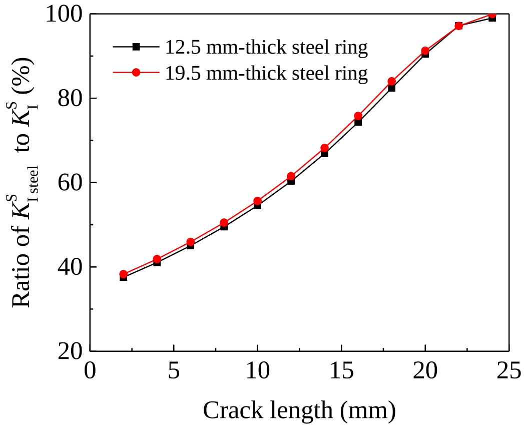

(e) Specimens c-t&b-12.5/19.5-50

(f) Specimens e-t&b-12.5/19.5-50

Fig. 10. Ratio of $K^{\mathrm{S}}_{\mathrm{I\,steel}}$ to $K^{\mathrm{S}}_{\mathrm{I}}$ in crack propagation process

Table 2. Ratios of $K^{\mathrm{S}}_{\mathrm{I\,steel}}/K^{\mathrm{S}}_{\mathrm{I}}$ at the cracking ages

Drying direction	Height (mm)	Steel ring thickness (mm)	Ratio of $K^{\mathrm{S}}_{\mathrm{I\,steel}}/K^{\mathrm{S}}_{\mathrm{I}}$	
			Circular	Elliptical
Outer surface	37.5	12.5	18.95%	16.82%
		19.5	15.16%	16.27%
Top & bottom surfaces	50	12.5	36.19%	37.54%
		19.5	38.41%	38.29%
	30	12.5	43.41%	46.53%
		19.5	44.71%	46.76%

5. Conclusions

The purpose of this study was to investigate the influence of the specimen geometry, steel ring thickness and boundary conditions on the cracking of concrete in the restrained elliptical ring test for assessing cracking tendency of concrete and other cement-based materials. A series of restrained circular and elliptical ring specimens with different steel ring thickness were tested under two drying conditions (from the outer circumferential surface and the top & bottom surfaces). A numerical method of the fracture mechanics was proposed to predict the entire fracture process in the concrete ring under restrained shrinkage. By comparison of concrete cracking ages under different drying and restraint conditions, the effects of ring geometry, steel ring thickness and drying condition on the crack initiation and propagation were discussed. Based on the experimental and numerical investigations, the following conclusions can be drawn:

(a) The drying condition has a significant effect on the fracture process of a concrete ring. In the case of drying from the outer circumferential surface, the crack initiates at the outer circumferential surface and propagates towards the inner surface of a concrete ring specimen. By contrast, in the case of drying from top & bottom surfaces, the crack initiates partially at the inner circumference of the concrete ring and propagates along the radial direction. The fracture process continues until the crack finally propagates throughout the ring wall. For both the circular and elliptical specimens, complete development of the cracks would occur immediately after the crack initiated or at most, in the period of about 1 day.

(b) Compared with traditional restrained circular ring specimens, the elliptical ring geometry has the advantage of improving the restraining effect and accelerating the occurrence of the first crack. In addition, the first crack occurs at a known location near the major radius in an elliptical concrete ring instead of a random position along the circumference in a circular concrete ring, making the determination of crack position more convenient. For both circular and elliptical ring specimens, a thicker steel ring can improve the restraining effect compared with a thinner steel ring. It should, however, be noted that this improvement was more obvious for circular rings and proves that the advantage of the elliptical ring is mainly caused by its geometrical shape.

(c) The driving forces to enable crack initiation and propagation come from two parts, namely the restraint from the inner steel ring and self-restraint caused by the non-uniform shrinkage of concrete. Using the moisture fields derived from a previous experimental study, the proportion of the restraint from steel ring was calculated to be less than 50% of total restraint, indicating that the fracture is not dominated by the restrained shrinkage but instead by the self-restraint caused by the non-uniform shrinkage in concrete. To clearly clarify the fracture mechanism of the ring test, it is significant to analyze the effect of the non-uniform shrinkage in concrete by introducing an effective moisture diffusion model.

Acknowledgement

The financial support of the National Natural Science Foundation of China under the grants of NSFC 51478083 and NSFC 51109026, UK Engineering and Physical Sciences Research Council under the grant of EP/I031952/1, and the National Basic Research Program of China (973 Program) under the grant of 2015CB057703 is gratefully acknowledged.

References:

[1] K. Kovler, Testing system for determining the mechanical behaviour of early age concrete under restrained and free uniaxial shrinkage, Mater. Struct. 27(6) (1994) 324-330.

[2] S.A. Altoubat, D.A. Lange, Creep, Shrinkage, and cracking of restrained concrete at early age, ACI Mater. J. 98(4) (2001) 323-331.

[3] R.I. Gilbert, Shrinkage cracking in fully restrained concrete members, ACI Mater. J. 89(6) (1992) 141-149.

[4] W.J. Weiss, W. Yang, S.P. Shah, Shrinkage cracking of restrained concrete slabs, J. Eng. Mech. 124(7) (1998) 765-774.

[5] W. Yang, W.J. Weiss, S.P. Shah, Predicting shrinkage stress field in concrete slab on elastic subgrade, J. Eng. Mech. 126(1) (2000) 35-42.
[6] J.G. Sanjayan, F. Collins, Numerical modeling of alkali-activated slag concrete beams subjected to restrained shrinkage, ACI Struct. J. 97(5) (2000) 594-602.
[7] F. Collins, J.G. Sanjayan, Cracking tendency of alkali-activated slag concrete subjected to restrained shrinkage, Cem. Concr. Res. 30(5) (2000) 791-798.
[8] W.J. Weiss, W. Yang, S.P. Shah, Influence of specimen size/geometry on shrinkage cracking of rings, J. Eng. Mech. 126(1) (2000) 93-101.
[9] S.W. Dean, A. Radlinska, B. Bucher, et al., Comments on the interpretation of results from the restrained ring test, J. ASTM Int. 5(10) (2008) 1-12.
[10] J. Zhang, G. Yuan, Y. Han, Evaluation of shrinkage induced cracking in early age concrete: from ring test to circular column, Int. J. Damage Mech. 26(5) (2015) 771-797.
[11] A. Passuello, G. Moriconi, S.P. Shah, Cracking behavior of concrete with shrinkage reducing admixtures and PVA fibers, Cement Concr. Compos. 31(10) (2009) 699-704.
[12] M.A. Miltenberger, E.K. Attiogbe, H.T. See, Shrinkage cracking characteristics of concrete using ring specimens, ACI Mater. J. 100(3) (2003) 239-245.
[13] J.H. Moon, F. Rajabipour, B. Pease, et al., Quantifying the influence of specimen geometry on the results of the restrained ring test, J. ASTM Int. 3(3) (2006) 1-14.
[14] W. Dong, X. Zhou, Z. Wu, A fracture mechanics-based method for prediction of cracking of circular and elliptical concrete rings under restrained shrinkage, Eng. Fract. Mech. 131(2014) 687-701.
[15] X. Zhou, W. Dong, O. Oladiran, Experimental and numerical assessment of restrained shrinkage cracking of concrete using elliptical ring specimens, J Mater. Civil Eng. 26(11) (2014) 04014087.
[16] H. Zhen, X.M. Zhou, Z.J. Li, New experimental method for studying early-age cracking of cement-cased materials, ACI Mater. J. 101(1) (2004) 50-56.
[17] W. Dong, X.M. Zhou, Z.M. Wu, et al., Quantifying the influence of elliptical ring geometry on the degree of restraint in a ring test, Comput. Struct. (2018) In press.
[18] W. Dong, X. Zhou, Z. Wu, et al., Investigating crack initiation and propagation of concrete in restrained shrinkage circular/elliptical ring test, Mater. Struct. 50(1) (2017) 1-13.
[19] W. Dong, X. Zhou, Z. Wu, et al., Effects of specimen size on assessment of shrinkage cracking

of concrete via elliptical rings: Thin vs. thick, Comput. Struct. 174 (2016) 66-78.

[20] W. Dong, W. Yuan, X. Zhou, et al., The fracture mechanism of circular/elliptical concrete rings under restrained shrinkage and drying from top and bottom surfaces, Eng. Fract. Mech. 189 (2017) 148-163.

[21] A.B. Hossain, J. Weiss, Assessing residual stress development and stress relaxation in restrained concrete ring specimens, Cement Concr. Compos. 26(5) (2004) 531-540.

[22] W.J. Weiss, S.P. Shah, Restrained shrinkage cracking: the role of shrinkage reducing admixtures and specimen geometry, Mater. Struct. 35(2) (2002) 85-91.

[23] A.B. Hossain, J. Weiss, The role of specimen geometry and boundary conditions on stress development and cracking in the restrained ring test, Cem. Concr. Res. 36(1) (2006) 189-199.

[24] A.M. Soliman, M.L. Nehdi, Effects of shrinkage reducing admixture and wollastonite microfiber on early-age behavior of ultra-high performance concrete, Cement Concr. Compos. 46(4) (2014) 81-89.

[25] D.Y. Yoo, J.J. Park, S.W. Kim, et al., Influence of ring size on the restrained shrinkage behavior of ultra high performance fiber reinforced concrete, Mater. Struct. 47(7) (2014) 1161-1174.

[26] J.H. Moon, J. Weiss, Estimating residual stress in the restrained ring test under circumferential drying, Cement Concr. Compos. 28(5) (2006) 486-496.

[27] A. Hillerborg, M. Modéer, P.E. Petersson, Analysis of crack formation and crack growth in concrete by means of fracture mechanics and finite elements, Cem. Concr. Res. 6(6) (1976) 773-781.

[28] P.E. Petersson, Crack growth and development of fracture zones in plain concrete and similar materials, Report TVBM-1006. Sweden: Division of Building Materials, Lund Institute of Technology (1981).

[29] W. Dong, X. Zhou, Z. Wu, On fracture process zone and crack extension resistance of concrete based on initial fracture toughness, Constr. Build. Mater. 49(6) (2013) 352-363.

[30] W. Dong, Z. Wu, X. Zhou, Calculating crack extension resistance of concrete based on a new crack propagation criterion, Constr. Build. Mater. 38(2) (2013) 879-889.

[31] K. Kovler, Drying creep of concrete in terms of the age-adjusted effective modulus method, Mag. Concrete Res. 49(181) (1997) 345-351.